ARTICLE IN PRESS

Available online at www.sciencedirect.com

SCIENCE DIRECT

Composites Science and Technology □ (□□□□) □–□

COMPOSITES SCIENCE AND TECHNOLOGY

www.elsevier.com/locate/compscitech

Composite laminate failure analysis using multicontinuum theory

J. Steven Mayes*[,1a], Andrew C. Hansen[b]

[a]Division of Mechanical Engineering, Alfred University, Alfred, NY 14802, USA
[b]Department of Mechanical Engineering, University of Wyoming, Laramie, WY 82071, USA

Received 1 August 1999; accepted 1 March 2003

Abstract

Damage in a composite material typically begins at the constituent level and may, in fact, be limited to only one constituent in some situations. An accurate prediction of constituent damage at sampling points throughout a laminate provides a genesis for progressively analyzing failure of a composite structure from start to finish. Multicontinuum Theory is a micromechanics based theory and associated numerical algorithm for extracting, virtually without a time penalty, the stress and strain fields for a composites' constituents during a routine finite element analysis. A constituent stress-based failure criterion is used to construct a nonlinear progressive failure algorithm for investigating the material failure strengths of composite laminates. The proposed failure analysis methodology was used to simulate the nonlinear laminate behavior and progressive damage of selected laminates under both uniaxial and biaxial load conditions up to their ultimate strength. This effort was part of a broader project to compare the predictive capability of current composite failure criteria.

Keywords: Multicontinuum

1. Introduction

A majority of failure criteria developed for composite materials to date can be classified as macromechanical because the criteria attempt to predict failure using composite stress–strain data. A key element of macromechanics is the combining of constituent's properties into a homogeneous set of composite lamina properties and possibly combining lamina properties into homogeneous laminate properties.

In contrast, micromechanical failure analyses retain the individual identities of each lamina and its constituents, thereby allowing interaction among them. Composite properties are utilized in micromechanics analyses but failure of each constituent and its contribution to lamina and laminate failure is emphasized. All micromechanical models are predicated on a complete set of material constants for each constituent that are consistent with those of the composite they form. This consistency is typically synthesized from a finite element or closed form analytical model of the composite microstructure. Examples of micromechanical approaches can be found in Aboudi [1], Pecknold [2], Rahman [3], and Kwon [4]. A review of these approaches can be found in Mayes [5].

2. Multicontinuum theory

Multicontinuum Theory (MCT) is a micromechanics based theory and associated numerical algorithm for extracting, virtually without a time penalty, the stress and strain fields for a composites' constituents during a routine finite element analysis. MCT development is presented in detail for linear-elastic and linear-viscoelastic composite behavior in papers by Garnich and Hansen[6,7]. The elasticity theory is summarized here to emphasize concepts important to implementing a constituent based failure analysis. The present theory assumes: (1) linear elastic behavior of the fibers and nonlinear elastic behavior of the matrix, (2) perfect bonding between the fibers and matrix, (3) stress concentrations at fiber boundaries are accounted for only as

* Corresponding author.
[1] Formerly of the Naval Surface Warfare Center, Carderock Division, Structures and Composites Department, West Bethesda, MD, USA.

0266-3538/$ - see front matter
doi:10.1016/S0266-3538(03)00219-7

Nomenclature

$\pm$	Indicates the appropriate tensile or compressive value is used depending on the constituent's stress state.
$\{a\}$	Vector relating constituent to composite thermal strains.
$[A]$	Matrix relating constituent to composite mechanical strains.
CTE	Coefficient of thermal expansion.
$[C]$	Composite stiffness matrix.
$[C_\beta]$	Constituent β stiffness matrix [$\beta = f$ (fiber), m (matrix)].
F_i, F_{ij}	Strength parameters (i,j = 1–6).
I_i	Composite transversely isotropic stress invariants (i = 1–5).
$I_{i\beta}$	Constituent β transversely isotropic stress invariants (i = 1–5).
$^{\pm}K_{i\beta}$	Constituent β failure parameter [$\beta = f$ (fiber), m (matrix)]; (i = 1–4).
$^{\pm}S_{ij\beta}$	Constituent β strength in the i,j direction [$\beta = f$ (fiber), m (matrix)]; (i,j = 1–3).
$^{\pm kl}S_{ij\beta}$	Constituent β stress in the i,j direction when stress $^{\pm}S_{kl}$ is applied [$\beta = f$ (fiber), m (matrix)]; (i,j = 1–3); (k,l = 1–3).
V	Volume.
$\{\alpha\}$	Composite coefficients of thermal expansion.
$\{\alpha_{ii\beta}\}$	Constituent β coefficients of thermal expansion [$\beta = f$ (fiber), m (matrix)]; (i = 1, 2).
$\tilde{\varepsilon}$	Composite strain tensor.
$\{\epsilon\}$	Composite total strain tensor in contracted (matrix) notation.
$\tilde{\varepsilon}_\beta$	Constituent β strain tensor [$\beta = f$ (fiber), m (matrix)].
$\{\epsilon_\beta\}$	Constituent β total strain tensor in contracted notation [$\beta = f$ (fiber), m (matrix)].
$\{\epsilon_o\}$	Composite thermal strain tensor in contracted notation.
$\{\epsilon_{\beta o}\}$	Constituent β thermal strain tensor in contracted notation [$\beta = f$ (fiber), m (matrix)].
ϕ_β	Constituent β volume fraction [$\beta = f$ (fiber), m (matrix)].
$\tilde{\sigma}$	Composite stress tensor.
$\{\sigma\}$	Composite stress tensor in contracted notation.
σ_{ij}	Composite stresses referenced to the lamina (i,j = 1–3) or laminate (i,j = x to z) coordinate system.
$\tilde{\sigma}_\beta$	Constituent β stress tensor [$\beta = f$ (fiber), m (matrix)].
$\{\sigma_\beta\}$	Constituent β stress tensor in contracted notation [$\beta = f$ (fiber), m (matrix)].
$\sigma_{ij\beta}$	Constituent β stresses referenced to the lamina coordinate system [$\beta = f$ (fiber), m (matrix)]; (i,j = 1 to 3).
ΔT	Difference between current and reference temperatures.
[1]	Identity matrix.

a contribution to the volume average stress, (4) the effect of fiber distribution on the composite stiffness and strength is accounted for in the finite element modeling of a representative volume of microstructure, and (5) ability to fail one constituent while leaving the other intact results in a piecewise continuous composite stress–strain curve.

MCT begins with a continuum definition of stress at a point. The concept of stress in homogeneous materials, such as steel, is a familiar one to most engineers. Yet, if looked at on a microscale, one sees that the "homogeneous" material is hardly homogeneous. It is obvious that stresses will vary significantly from point to point across different phases and inclusions. The homogenized value used to characterize the stress tensor at a point in a single continuum material is derived by taking a volume average of all stresses in the region as

$$\tilde{\sigma} = \frac{1}{V}\int_D \tilde{\sigma}(\mathbf{x})\mathrm{d}V, \tag{1}$$

where D is the region representing the continuum point. The concept of a multicontinuum simply extends this concept to reflect coexisting materials within a continuum point. In particular, consider a composite material with two clearly identifiable constituents as shown in Fig. 1 [8]. Using Eq. (1) for each constituent we can write:

$$\tilde{\sigma}_f = \frac{1}{V_f}\int_{D_f} \tilde{\sigma}(\mathbf{x})\mathrm{d}V, \tag{2}$$

and

$$\tilde{\sigma}_m = \frac{1}{V_m}\int_{D_m} \tilde{\sigma}(\mathbf{x})\mathrm{d}V, \tag{3}$$

where

$$D = D_f \bigcup D_m. \tag{4}$$

Combining Eqs. (1)–(3) leads to

$$\tilde{\sigma} = \phi_f\tilde{\sigma}_f + \phi_m\tilde{\sigma}_m, \tag{5}$$

where ϕ_f and ϕ_m are the volume fractions of fiber and matrix respectively. Likewise, for strains we have

$$\tilde{\varepsilon} = \phi_f\tilde{\varepsilon}_f + \phi_m\tilde{\varepsilon}_m. \tag{6}$$

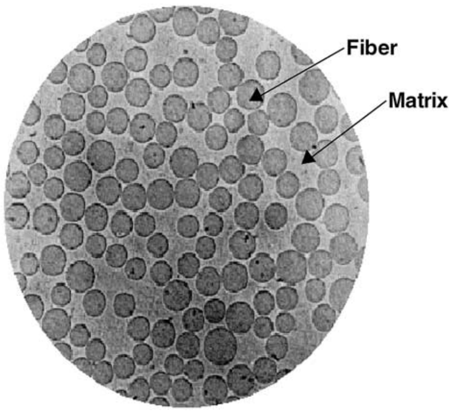

Fig. 1. Composite lamina as a multicontinuum.

It is important to note the averaging process that results in these equations. That is, we are not concerned with stress and strain variations through individual constituents within D but only with their average values. This is an information compromise that separates structural analysis from micromechanical analysis. Accounting for stress variations throughout every fiber at every material point in even a modest structure is simply not possible or desirable. In contrast, providing constituent average stress and strain fields opens a new and manageable information window on a composite material's response to a load.

Changing from direct tensor to contracted matrix notation, the elastic constitutive laws for the composite and the constituents are given by

$$\{\sigma\} = [C](\{\varepsilon\} - \{\varepsilon_o\}), \tag{7}$$

$$\{\sigma_f\} = [C_f](\{\varepsilon_f\} - \{\varepsilon_{fo}\}), \tag{8}$$

and

$$\{\sigma_m\} = [C_m](\{\varepsilon_m\} - \{\varepsilon_{mo}\}). \tag{9}$$

Combining Eqs. (5)–(9), constituent fiber and matrix strain fields, $\{\varepsilon_f\}$and $\{\varepsilon_m\}$ respectively, are derived from the composite strain field $\{\epsilon\}$ using

$$\{\varepsilon_m\} = (\phi_m[1] + \phi_f[A])^{-1}(\{\varepsilon\} - \Delta T\{a\}), \tag{10}$$

and

$$\{\varepsilon_f\} = \frac{1}{\phi_f}(\{\varepsilon\} - \phi_m\{\varepsilon_m\}), \tag{11}$$

where

$$[A] = -\frac{\phi_m}{\phi_f}([C] - [C_f])^{-1}([C] - [C_m]),$$

and

$$\{a\} = ([C] - [C_f])^{-1}([C]\{\alpha\} - \phi_f[C_f]\{\alpha_f\} - \phi_m[C_m]\{\alpha_m\}).$$

An isothermal version of Eq. (10) appeared in early work by Hill [9]. Typically $[C_f]$, $[C_m]$, $\{\alpha_f\}$, and $\{\alpha_m\}$, are developed from known material properties of the constituents, while $[C]$ and $\{\alpha\}$ of the composite are developed from micromechanical modeling of an assumed fiber-matrix distribution incorporating the constituent material properties. Hence, $[A]$ and $\{a\}$ are known a priori to a structural analysis. A major advantage of a MCT analysis is the increased computational efficiency gained by the theory's decoupling of micromechanical modeling from structural analysis.

MCT's ability to calculate accurate constituent stress and strain fields is dependent on constituent elastic constants derived from experimentally determined composite values. Further, MCT's ability to execute realistic failure analysis is dependent on accurate values for constituent strength parameters, also derived from experimentally determined composite values. The link establishing a relationship between composite (macro) and constituent (micro) elastic constants is a finite element micromechanics model for a continuous fiber unidirectional composite. The finite element micromechanics model used in this research was advanced by Garnich [10] which contains discussion of its development. Only major components of the model will be summarized here.

The micromechanics model is based on an assumption of uniform hexagonal fiber packing within the lamina's matrix (Fig. 2). A unit cell, representative of the repeating microstructure, is extracted from a region bounded by symmetry lines. Unit cell geometry, fiber volume fraction, and boundary conditions are used to define the finite element model (Fig. 3). The unit cell is based on a generalized plane strain assumption in the fiber direction but is fully three-dimensional. The cell is modeled with a finite element scripting language allowing material properties and fiber volume fraction to be varied as required. Boundary conditions [10,11] necessary to enforce compatibility of unit cell boundaries with adjacent unit cells are generated automatically. Four linear elastic load cases are solved (longitudinal tension, transverse tension, transverse shear, and long-

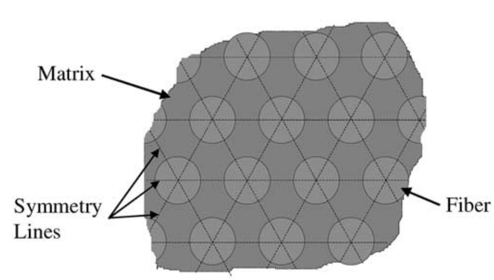

Fig. 2. Idealized lamina microstructure.

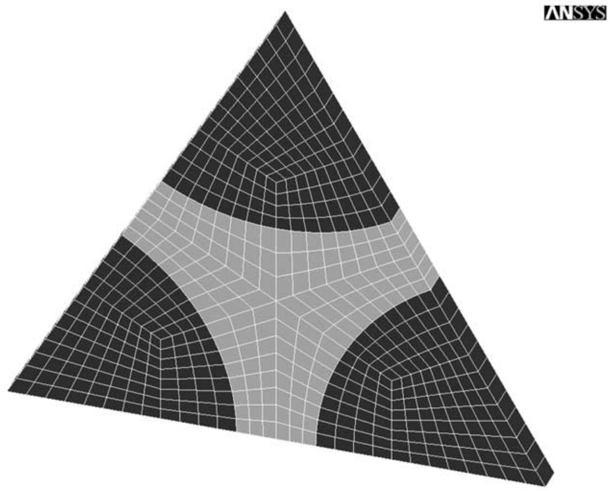

Fig. 3. Finite element model of a unit cell created using the ANSYS software.

itudinal shear) to determine and verify five independent elastic constants for transversely isotropic composite lamina.

All constituent elastic constants (Tables 1 and 2) and strengths (Tables 3 and 4) were backed out via the micromechanics model from experimentally determined composite values provided by the organizers [12]. These in situ constituent values used in the MCT analyses conducted herein were different than those presented for this exercise by the organizers.

3. Failure criterion

The Maximum Distortional Energy, or von Mises, criterion is the most widely used criterion for predicting yield points in isotropic metals[13]. The isotropic von Mises failure criterion is a special case of a general form of quadratic interaction criteria, so named because they include terms to account for interaction between the stress components. Variations of the general criteria have been used to predict brittle failure in orthotropic materials[14].

A generalized quadratic interaction failure criterion, suggested by Gol'denblat and Kopnov [15] and proposed by Tsai and Wu[16], is given as

$$F_i\sigma_i + F_{ij}\sigma_i\sigma_j = 1, \tag{12}$$

where F_i and F_{ij} are experimentally determined strength tensors and contracted tensor notation is used ($i,j = 1$–6). Hoffman [17] has suggested that the linear terms, F_i, are necessary to account for differences in tensile and compressive strengths whereas Tsai and Wu state that they are necessary to account for internal stresses. Tsai and Wu [16] presented a form of Eq. (12) for transversely isotropic composites as

$$\begin{aligned} &F_1\sigma_{11} + F_2(\sigma_{22}+\sigma_{33}) + F_{11}\sigma_{11}^2 + F_{22}\left(\sigma_{22}^2+\sigma_{33}^2+2\sigma_{23}^2\right) \\ &+ F_{66}\left(\sigma_{12}^2+\sigma_{13}^2\right) \\ &+ 2F_{12}(\sigma_{11}\sigma_{22}+\sigma_{11}\sigma_{33}) + 2F_{23}\left(\sigma_{22}\sigma_{33}-\sigma_{23}^2\right) = 1. \end{aligned} \tag{13}$$

Hashin [18] developed a three-dimensional, stress interactive, failure criterion for unidirectional lamina that recognized two distinct and uncoupled failure modes. While the failure criterion itself was based on composite stresses, it constructs a piecewise continuous failure form based on constituent failure modes. The failure criterion assumes transverse isotropy for a unidirectional composite. A local orthogonal coordinate system is defined in which the fiber axis serves as the principal, x_1, material direction, and x_2, x_3 the trans-

Table 1
Matrix elastic constants calculated from micromechanics

Matrix	E_m (GPa)	G_m (GPa)	ν_m	α_m (10^{-6}/°C)
3501-6	4.50	1.68	0.340	35
BSL914C	4.50	1.68	0.340	35
LY556/HT907/DY063	4.95	1.83	0.355	52
MY750/HY917/DY063	4.85	1.78	0.360	49

Table 3
Matrix strengths calculated from micromechanics

Matrix	$^{+}S_{22m}$ (MPa)	$^{-}S_{22m}$ (MPa)	$^{+22}S_{33m}$ (MPa)	$^{-22}S_{33m}$ (MPa)	S_{12m} (MPa)
3501-6	42.3	−176.3	5.52	−23.0	49.54
BSL914C	23.2	−172.2	2.73	−20.2	50.8
LY556/HT907/DY063	27.3	−88.9	4.26	−13.9	44.9
MY750/HY917/DY063	31.5	−114.3	4.63	−16.8	46.3

Table 2
Fiber elastic constants calculated from micromechanics

Fiber	E_{11f} (GPa)	E_{22f} (GPa)	G_{12f} (GPa)	G_{23f} (GPa)	ν_{12f}	ν_{23f}	α_{11f} (10^{-6}/°C)	α_{22f} (10^{-6}/°C)
AS4	207.5	25.0	95.0	9.20	0.240	0.359	−1.7	15
T300	227.0	25.0	28.0	9.50	0.245	0.316	−1.7	15
E-glass 21xK43 Gevetex	83.2	83.2	33.5	33.5	0.240	0.240	6.9	6.9
Silenka E-glass 1200tex	73.0	73.0	29.6	29.6	0.235	0.235	6.6	6.6

Table 4
Fiber strengths calculated from micromechanics

Fiber	$^{+}S_{11f}$ (MPa)	$^{-}S_{11f}$ (MPa)	S_{12f} (MPa)
AS4	3202	−2431.	101
T300	2466	−1480.	105
E-glass 21xK43 Gevetex	1772	−886.	93.0
Silenka E-glass 1200tex	2040	−1275.	95.2

verse and through-thickness directions. The failure state of the material is expressed in terms of transversely isotropic stress invariants. Although Hashin derived these invariants, Hansen [19], in development of an anisotropic flow rule for plastic behavior in composite materials, presented a different form used within this paper. The five transversely isotropic stress invariants are:

$$\begin{aligned}
I_1 &= \sigma_{11} \ , \\
I_2 &= \sigma_{22} + \sigma_{33} \ , \\
I_3 &= \sigma_{22}^2 + \sigma_{33}^2 + 2\sigma_{23}^2 \ , \\
I_4 &= \sigma_{12}^2 + \sigma_{13}^2 \ , \\
I_5 &= \sigma_{22}\sigma_{12}^2 + \sigma_{33}\sigma_{13}^2 + 2\sigma_{12}\sigma_{13}\sigma_{23} \ .
\end{aligned} \tag{14}$$

Hashin's choice of a quadratic form eliminates I_5 from appearing in the failure criterion. Therefore the most general form for a quadratic criterion [18] is

$$K_1I_1 + L_1I_1^2 + K_2I_2 + L_2I_2^2 + M_{12}I_1I_2 + K_3I_3 + K_4I_4 = 1, \tag{15}$$

where K_i, L_i, and M_{12} are experimentally determined failure coefficients.

At this point, it is instructive to compare the criterion of Tsai and Wu with that of Hashin. Rewriting Eq. (13) in terms of the transversely isotropic stress invariants gives

$$F_1I_1 + F_2I_2 + F_{11}I_1^2 + F_{22}I_3 + F_{66}I_4 + 2F_{12}I_1I_2 + 2F_{23}\left(I_2^2 - I_3\right) = 1,$$

or rearranging,

$$F_1I_1 + F_{11}I_1^2 + F_2I_2 + 2F_{23}I_2^2 + 2F_{12}I_1I_2 + (F_{22} - 2F_{23})I_3 + F_{66}I_4 = 1. \tag{16}$$

Comparing Eq. (16) to Eq. (15), shows that the Tsai–Wu criterion for transversely isotropic materials and the Hashin failure criterion have the same functional form. Their difference is in defining the coefficients of the stress terms. The Tsai–Wu equation is used to define a smooth and continuous failure surface in both the tension and compression regions of space. As a result the coefficients are functions of both tensile and compressive composite strengths. In contrast, Hashin identified two composite failure modes; fiber versus matrix influenced, and developed separate equations based on the failure mode to determine a failure state. Hashin further recognized that a composite typically has different ultimate strengths in tension and compression, so both fiber and matrix failure criteria have tensile and compressive subforms. Hence the coefficients of the stress terms are functions of only tension or compression strengths resulting in a piecewise continuous stress-space failure surface.

In what follows, we adopt the view of Hashin and develop separate failure criteria for the fiber and matrix failure modes. However, in a major departure from Hashin's work, we develop failure criteria in the form of Eq. (15) for *each constituent* as opposed to the composite by utilizing constituent stress information produced by MCT. As a consequence, the transversely isotropic stress invariants, defined in Eq. (14), were used for each constituent of the composite material under consideration. Furthermore, recognizing that constituents typically have different ultimate strengths in tension and compression, each constituent failure criterion has a tensile and compressive subform.

A unique aspect of the MCT failure theory is that an anisotropic failure theory is used on an isotropic matrix material. This complexity is necessitated by the fact that the matrix failure behavior will be anisotropic due to microstructural geometry. The root of this phenomenon can be conceptualized by considering a transversely isotropic unidirectional composite. If all fibers were removed but their holes retained only a matrix of "Swiss Cheese" would remain. Because of the remaining microstructure, macroscopic failure of the material will be fundamentally

Table 5
Nonlinear shear curve fit parameters

Composite	B_0 (Pa)	B_1 (Pa)	B_2 (Pa)	h_1	h_2
AS4/3501-6	3.31E+14	−1.09E+14	4.39E+14	−0.0536	−0.0132
T300/BSL914C	1.64E+11	−1.51E+8	−1.63E+11	−43.7	0.00654
E-glass/LY556/HT907/DY063	5.76E+10	−9.51E+7	−5.75E+10	−71.9	0.00706
E-glassMY750/HY917/DY063	2.69E+10	−9.961E+7	−2.68E+10	−63.1	0.0161

different in axial versus transverse directions resulting in a transversely isotropic failure envelope.

As a first approximation, we would like to simplify Eq. (15) for each of the constituents. Pipes and Cole[20] demonstrated some of the difficulties in experimentally determining stress interaction terms such as M_{12}, analogous to F_{12} in the Tsai–Wu theory. Further, Narayanaswami [21] demonstrated numerically that setting the stress interaction term F_{12} to zero in the Tsai-Wu quadratic failure criterion in plane stress analyses resulted in less than 10% error for all the load cases and materials considered. Hence, we set M_{12} equal to zero. Tsai and Wu identify the linear terms in Eq. (13) as necessary to account for internal stresses. Internal stresses refer to self equilibrating stresses within each constituent which, when added together according to Eq. (5), produce no composite stress. Internal stresses may arise in composites operating at a temperature other than the reference temperature due to a mismatch in constituent coefficients of thermal expansion. These internal stresses are accounted for in the formulation of Multicontinuum Theory through the $\{a\}$ vector. Thus we eliminate the linear terms from Eq. (15). If analytical comparisons against experimental results do not provide a satisfactory correlation, these terms, along with the term M_{12}, could be reexamined for their potential contributions.

Noting the above, the general form for a stress interactive failure criterion, after changing to a consistent coefficient notation, is given by

$$K_1 I_1^2 + K_2 I_2^2 + K_3 I_3 + K_4 I_4 = 1. \tag{17}$$

Developing a form of Eq. (17) for fiber failure we note that the majority of fibers used for composite reinforcement have greater transverse strengths than the matrices commonly used in conjunction with them. Hence, we assume that transverse failure of these composites is matrix dominated. Based on this assumption, we set K_2 and K_3 equal to zero in Eq. (17) as their associated stress invariants involve transverse normal stresses. The fiber failure criterion reduces to

$$K_{1f} I_{1f}^2 + K_{4f} I_{4f} = 1. \tag{18}$$

To determine coefficients for each stress term, we solve Eq. (18) considering individual load cases of pure in-plane shear, tension, and compression applied to unidirectional lamina. For the case of in-plane shear load only ($\sigma_{12f}\, 0, \neq \sigma_{11f} = 0$), we find

$$K_{4f} = \frac{1}{S_{12f}^2},$$

where, S_{12f} denotes fiber shear strength. For the case of tensile load only ($\sigma_{11f} > 0$; $\sigma_{12f} = 0$), we find

$$^{+}K_{1f} = \frac{1}{^{+}S_{11f}^2}.$$

For the case of compression load only ($\sigma_{11f} < 0$; $\sigma_{12f} = 0$), we find

$$^{-}K_{1f} = \frac{1}{^{-}S_{11f}^2}.$$

The criterion for fiber failure can now be expressed as

$$^{\pm}K_{1f} I_{1f}^2 + K_{4f} I_{4f} = 1. \tag{19}$$

The $\pm$symbol indicates that the appropriate tensile or compressive ultimate strength value is used depending on the constituent's stress state.

To determine the coefficients of Eq. (17) for matrix failure we first solve the equation considering load cases of pure in-plane and transverse shear. For the case of transverse shear only ($\sigma_{23m} \neq 0$, $\sigma_{11m} = \sigma_{22m} = \sigma_{33m} = \sigma_{12m} = 0$), we find

$$K_{3m} = \frac{1}{2S_{23m}^2}.$$

For the case of in-plane shear only ($\sigma_{12m} \neq 0$, $\sigma_{11m=}\sigma_{22m} = \sigma_{33m} = \sigma_{23m} = 0$), we find

$$K_{4m} = \frac{1}{S_{12m}^2}.$$

Noting that a majority of fibers used for composite reinforcement have greater longitudinal strengths than the matrices commonly used in conjunction with them, we assume that the longitudinal failure of these composites is fiber dominated. Based on this assumption and some numerical sensitivity studies we set K_{1m} equal to zero. The approach to our 'sensitivity analysis' was to conduct failure analyses, with and without parameter K_{1m} in the proposed failure criteria, on all available test cases. We determined that the presence of K_{1m} did not significantly affect failure predictions results for those cases. Incorporating these results into (17) gives

$$K_{2m} I_{2m}^2 + \frac{1}{2S_{23m}^2} I_{3m} + \frac{1}{S_{12m}^2} I_{4m} = 1. \tag{20}$$

To determine K_{2m}, we consider the case of transverse tensile load only ($(\sigma_{22m} + \sigma_{33m}) > 0$, $\sigma_{23m} = \sigma_{12m} = 0$) and find

$$^{+}K_{2m} = \frac{1}{(^{+}S_{22m} + {}^{+22}S_{33m})^2}\left(1 - \frac{^{+}S_{22m}^2 + {}^{+22}S_{33m}^2}{2S_{23m}^2}\right).$$

The numeric superscripts ("22") in the above failure parameters are used to denote the direction of the applied load. Note that while a pure transverse (one-dimensional) load, σ_{22}, on a composite lamina results in

$$\sigma_{11} = \sigma_{33} = 0,$$

the constituents experience a fully three-dimensional stress state[6,7]. Likewise, for the case of a pure transverse compressive load $[(\sigma_{22m} + \sigma_{33m}) < 0,\ \sigma_{23m} = \sigma_{12m} = 0]$

$${}^{-}K_{2m} = \frac{1}{({}^{-}S_{22m} + {}^{-22}S_{33m})^2}\left(1 - \frac{{}^{-}S_{22m}^2 + {}^{-22}S_{33m}^2}{2S_{23m}^2}\right).$$

The criterion for matrix failure can now be expressed as

$${}^{\pm}K_{2m}I_{2m}^2 + K_{3m}I_{3m} + K_{4m}I_{4m} = 1. \tag{21}$$

Transverse shear strength values were not provided as part of the material characterizations provided by the organizers [12]. Parameter ${}^{\pm}K_{2m}$ is highly sensitive to these values and rather than risk using inaccurate values, the matrix failure criterion was modified. Expanding Eq. (21) in terms of local stress components gives

$${}^{\pm}K_{2m}(\sigma_{22m} + \sigma_{33m})^2 + K_{3m}(\sigma_{22m}^2 + \sigma_{33m}^2 + 2\sigma_{23m}^2) + K_{4m}(\sigma_{12m}^2 + \sigma_{13m}^2) = 1.$$

For the load cases considered in this paper, no transverse shear stresses arise in the constituents so we set $\sigma_{23m} = 0$ and rearrange the above as

$$({}^{\pm}K_{2m} + K_{3m})\sigma_{22m}^2 + ({}^{\pm}K_{2m} + K_{3m})\sigma_{33m}^2 + {}^{\pm}K_{2m}(2\sigma_{22m}\sigma_{33m}) + K_{4m}(\sigma_{m12}^2 + \sigma_{13m}^2) = 1. \tag{22}$$

${}^{\pm}K_{2m}$ scales a stress interaction in the third term of Eq. (22). We set this scale factor to zero as was done previously in the simplification of Eq. (15). This results in

$${}^{\pm}K_{3m}(\sigma_{22m}^2 + \sigma_{33m}^2) + K_{4m}(\sigma_{12m}^2 + \sigma_{13m}^2) = 1.$$

Therefore, in terms of the transversely isotropic stress invariants, the modified matrix failure criterion becomes

$${}^{\pm}K_{3m}I_{3m} + K_{4m}I_{4m} = 1, \tag{23}$$

where

$${}^{\pm}K_{3m} = \frac{1}{{}^{\pm}S_{22m}^2 + {}^{\pm22}S_{33m}^2}.$$

The mode of failure, fiber or matrix, is determined by monitoring their failure criteria given by Eqs. (19) and (23), respectively. The relative contribution of the various stress components to initial, intermediate, and final failure states can be determined by examining the product of the failure parameter $K_{i\beta}$ and its associated stress invariant $I_{i\beta}$ (For examples, see Tables 6–12).

4. Description of analysis method

A numerical MCT algorithm, based on Eqs. (10) and (11), was developed and incorporated into an in-house finite element code [22]. While the finite element approach may be more powerful than necessary for the analyses conducted as part of this exercise, the methodology was originally developed for failure analyses of general composite structures. Using the finite element

Table 6
Initial E-glass/LY55/HT907/DY063 failure envelope summary for a $[90°/\pm30]_S$ laminate under biaxial, σ_y/σ_x, load

Point	Lamina	Primary term	Secondary term	Failure mode
a	±30	$K_{3m}I_{3m}=1.0$	$K_{4m}I_{4m}=0.0$	Matrix - tension
b	90	$K_{3m}I_{3m}=1.0$	$K_{4m}I_{4m}=0.0$	Matrix - tension
c	90	$K_{3m}I_{3m}=1.0$	$K_{4m}I_{4m}=0.0$	Matrix - tension
d	±30	$K_{3m}I_{3m}=0.66$	$K_{4m}I_{4m}=0.34$	Matrix - comp/shear
e	90	$K_{3m}I_{3m}=1.0$	$K_{4m}I_{4m}=0.0$	Matrix - compression

Table 7
Final E-glass/LY55/HT907/DY063 failure envelope summary for a $[90°/\pm30°]_S$ laminate under biaxial, σ_y/σ_x, load

Point	Lamina	Primary term	Secondary term	Failure mode
A	30	$K_{4f}I_{4f}=0.77$	$K_{1f}I_{1f}=0.33$	Fiber - comp/shear
B	90	$K_{1f}I_{1f}=1.0$	$K_{4f}I_{4f}=0.0$	Fiber - tension
C	±30	$K_{1f}I_{1f}=0.78$	$K_{4f}I_{4f}=0.22$	Fiber - tension/shear
D	90	$K_{1f}I_{1f}=1.0$	$K_{4f}I_{4f}=0.0$	Fiber - compression
E	90	$K_{1f}I_{1f}=1.0$	$K_{4f}I_{4f}=0.0$	Fiber - compression
	±30	$K_{4f}I_{4f}=0.83$	$K_{1f}I_{1f}=0.17$	Fiber - shear/tension
F	±30	$K_{3m}I_{3m}=0.66$	$K_{4m}I_{4m}=0.34$	Matrix - comp/shear
	90	$K_{1f}I_{1f}=1.0$	$K_{4f}I_{4f}=0.0$	Fiber - compression
G	±30	$K_{3m}I_{3m}=0.97$	$K_{4m}I_{4m}=0.03$	Matrix - compression
	90	$K_{1f}I_{1f}=1.0$	$K_{4f}I_{4f}=0.0$	Fiber – compression
H	90	$K_{3m}I_{3m}=1.0$	$K_{4m}I_{4m}=0.0$	Matrix – compression
	±30	$K_{4f}I_{4f}=0.71$	$K_{4f}I_{4f}=0.29$	Fiber - shear/comp

Table 8
Initial E-glass/LY55/HT907/DY063 failure envelope summary for a $[90°/\pm30°]_S$ laminate under biaxial, σ_x/σ_{xy}, load

Point	Lamina	Primary term	Secondary term	Failure mode
a	90	$K_{3m}I_{3m}=1.0$	$K_{4m}I_{4m}=0.0$	Matrix - compression
b	90	$K_{3m}I_{3m}=0.72$	$K_{4m}I_{4m}=0.28$	Matrix - comp/shear
	−30	$K_{3m}I_{3m}=0.95$	$K_{4m}I_{4m}=0.05$	Matrix – tension/shear
c	−30	$K_{3m}I_{3m}=1.0$	$K_{4m}I_{4m}=0.0$	Matrix - tension
d	90	$K_{3m}I_{3m}=1.0$	$K_{4m}I_{4m}=0.0$	Matrix - tension

Table 9
Final E-glass/LY55/HT907/DY063 failure envelope summary for a $[90°/\pm 30°]_S$ laminate under biaxial, σ_x/σ_{xy}, load

Point	Lamina	Primary term	Secondary term	Failure mode
A	+30	$K_{4f}I_{4f}=0.54$	$K_{1f}I_{1f}=0.46$	Fiber- shear/comp
B	90	$K_{3m}I_{3m}=0.72$	$K_{4m}I_{4m}=0.28$	Matrix- comp/shear
	−30	$K_{3m}I_{3m}=0.95$	$K_{4m}I_{4m}=0.05$	Matrix - tension
	−30	$K_{1f}I_{1f}=0.86$	$K_{4f}I_{4f}=0.14$	Fiber - comp/shear
	+30	$K_{4f}I_{4f}=0.98$	$K_{1f}I_{1f}=0.02$	Fiber - shear
C	−30	$K_{1f}I_{1f}=1.0$	$K_{4f}I_{4f}=0.0$	Fiber - compression
	90	$K_{4f}I_{4f}=0.91$	$K_{1f}I_{1f}=0.08$	Fiber - shear/tension
	+30	$K_{4f}I_{4f}=1.0$	$K_{1f}I_{1f}=0.0$	Fiber - shear
D	−30	$K_{1f}I_{1f}=1.0$	$K_{4f}I_{4f}=0.0$	Fiber- tension
E	+30	$K_{1f}I_{1f}=0.95$	$K_{4f}I_{4f}=0.05$	Fiber- tension
F	+30	$K_{4m}I_{4m}=0.72$	$K_{3m}I_{3m}=0.28$	Fiber- shear/tension
G	−30	$K_{4m}I_{4m}=0.61$	$K_{3m}I_{3m}=0.39$	Matrix - tension/shear
	+30	$K_{4f}I_{4f}=0.77$	$K_{1f}I_{1f}=0.23$	Fiber - shear/tension
H	+30	$K_{4f}I_{4f}=0.77$	$K_{1f}I_{1f}=0.23$	Fiber - shear/tension
	90	$K_{1f}I_{1f}=1.0$	$K_{4f}I_{4f}=0.0$	Fiber - tension

Table 10
Initial AS4/3501-6 failure envelope summary for a $[0°/90°/\pm 45°]_S$ laminate under biaxial, σ_y/σ_x, load

Point	Lamina	Primary term	Secondary term	Failure mode
a	All	$K_{3m}I_{3m}=1.0$	$K_{4m}I_{4m}=0.0$	Matrix- tension
b	90	$K_{3m}I_{3m}=1.0$	$K_{4m}I_{4m}=0.0$	Matrix- tension
c	90	$K_{3m}I_{3m}=1.0$	$K_{4m}I_{4m}=0.0$	Matrix- tension

Table 11
Final AS4/3501-6 failure envelope summary for a $[0°/90°/\pm 45°]_S$ laminate under biaxial, σ_y/σ_x, load

Point	Lamina	Primary term	Secondary term	Failure mode
A	All	$K_{1f}I_{1f}=1.0$	$K_{4f}I_{4f}=0.0$	Fiber - tension
B	0	$K_{1f}I_{1f}=1.0$	$K_{4f}I_{4f}=0.0$	Fiber - tension
	90	$K_{1f}I_{1f}=1.0$	$K_{4f}I_{4f}=0.0$	Fiber - tension
	±45	$K_{4f}I_{4f}=0.88$	$K_{1f}I_{1f}=0.22$	Fiber - shear/tension
C	±45	$K_{4f}I_{4f}=0.98$	$K_{1f}I_{1f}=0.02$	Fiber - shear/tension
D	0	$K_{1f}I_{1f}=1.0$	$K_{4f}I_{4f}=0.0$	Fiber - tension
	90	$K_{1f}I_{1f}=1.0$	$K_{4f}I_{4f}=0.0$	Fiber - compression
E	±45	$K_{4f}I_{4f}=1.0$	$K_{1f}I_{1f}=0.0$	Fiber - shear
	90	$K_{1f}I_{1f}=1.0$	$K_{4f}I_{4f}=0.0$	Fiber - compression
F	90	$K_{1f}I_{1f}=1.0$	$K_{4f}I_{4f}=0.0$	Fiber - compression
	±45	$K_{4f}I_{4f}=0.75$	$K_{1f}I_{1f}=0.25$	Fiber - shear/comp
G	90	$K_{1f}I_{1f}=1.0$	$K_{4f}I_{4f}=0.0$	Fiber - compression
	±45	$K_{4f}I_{4f}=0.66$	$K_{1f}I_{1f}=0.34$	Fiber - shear/comp
H	All	$K_{1f}I_{1f}=1.0$	$K_{4f}I_{4f}=0.0$	Fiber - compression

framework provides a high degree of analytical flexibility.

A majority of composite materials in use today have organic matrices that produce significant nonlinear shear stress–strain behavior as demonstrated by the shear stress–strain curves presented by the organizers[12]. For the research considered herein, unloading or sustained creep of the composite was not a consideration. Therefore, a nonlinear-elastic constitutive model, as developed by Mayes [22], relating changes in elastic constants due to changing composite shear modulus was used. The model uses a three-term exponential series of the form

Table 12
E-glass/MY750/HT917/DY063 failure envelope summary for a $[\pm 55°]_S$ laminate under biaxial, σ_y/σ_x, load

Point	Lamina	Primary term	Secondary term	Failure mode
A	±55	$K_{3m}I_{3m}=1.0$	$K_{4m}I_{4m}=0.0$	Matrix - tension
B	±55	$K_{3m}I_{3m}=.90$	$K_{4m}I_{4m}=0.10$	Matrix – tension/shear
C	±55	$K_{3m}I_{3m}=0.62$	$K_{4m}I_{4m}=0.38$	Matrix – tension/shear
D	±55	$K_{4m}I_{4m}=0.79$	$K_{3m}I_{3m}=0.21$	Matrix - shear/tension
	±55	$K_{4f}I_{4f}=0.86$	$K_{1f}I_{1f}=0.14$	Fiber - shear/comp
E	±55	$K_{4f}I_{4f}=0.61$	$K_{1f}I_{1f}=0.39$	Fiber - shear/comp
F	±55	$K_{3m}I_{3m}=0.87$	$K_{4m}I_{4m}=0.13$	Matrix - comp/shear
G	±55	$K_{3m}I_{3m}=0.69$	$K_{4m}I_{4m}=0.31$	Matrix - comp/shear
H	±55	$K_{4f}I_{4f}=0.96$	$K_{1f}I_{1f}=0.04$	Fiber - shear/tension

$$\tau = B_0 + B_1 e^{(h_1\gamma)} + B_2 e^{(h_2\gamma)}, \tag{24}$$

to fit in-plane experimentally determined composite shear stress–strain curves. B_i and h_i are curve fit parameters, τ is shear stress (Pa), and γ is engineering shear strain (dimensionless). Nonlinear regression was used to fit the five equation parameters to experimental shear data (Table 5). A strain dependent, tangent shear modulus was computed from the first derivative of Eq. (24) for use during a finite element analysis. Tension and compression elastic moduli for all lamina were assumed to be constant.

In the finite element method, numerical integration samples stress, strain, and material values at Gauss quadrature points. MCT failure analyses store a state variable corresponding to composite material damage for every Gauss point. Three composite material conditions or states, listed in increasing damage severity, are defined as:

1. undamaged composite,
2. composite damaged by matrix failure, and
3. composite damaged by fiber failure.

When either constituent fails, all its moduli are immediately reduced to a near zero value at that Gauss point. Near zero values are used rather than zero to avoid numerical difficulties. Matrix moduli are reduced to 1% of their original value. Fiber moduli, which are typically one to two orders of magnitude larger than matrix moduli, are reduced by whatever percentage is required to bring damaged fiber values to the same magnitude as damaged matrix so that near zero stiffness values are the same for both constituents. Poisson's ratios remain constant. Their values are rendered irrelevant by the use of near zero moduli values which scale elements of the stiffness matrix, $[C_\beta]$, to near zero values. Since all constituent properties, both intact and failed, are known a priori, the micromechanics model (Fig. 3) is used to determine two additional sets of composite properties, corresponding to damage states 2 and 3, before conducting a MCT failure analysis.

The nonlinear character of a failure analysis requires the load to be incrementally applied and the damage tracked progressively. Initially, composite material properties are set to an undamaged condition. At each load step a damage algorithm, using the failure criteria formulated in Eqs. (19) and (23), checks every Gauss point for constituent failure based on accumulative stresses. When constituent failure is detected at a Gauss point, stresses are recalculated using accumulated strains and updated material properties. Gradual softening of the structure due to composite damage at the Gauss points and a nonlinear-elastic constitutive model causes an equilibrium imbalance between the applied (external) and resisting (internal) load vectors. A standard Modified Newton–Raphson nonlinear iterative procedure within each load step calculates differences between external and internal load vectors and applies it to the structure as a ''virtual'' load. The net effect is to increase nodal displacements, hence Gauss point strains and stresses, until equilibrium is restored and the next load step is then applied.

Structural failure of a laminate is defined as that point in the load history when the structure can no longer support the accumulated load and deflections begin to grow without bound. Unbounded growth is detected during equilibrium iterations by monitoring changes in the Euclidean (L_2) norm of the structural displacement vector.

5. MCT simulations of load-response to failure for selected laminates

Unidirectional (UD) E-glass/LY556/HT907/DY063 and T300/BSL914C lamina failure envelopes under biaxial normal-shear loads are shown in Figs. 4 and 5. These failure envelopes were symmetric about the abscissa and showed a typical quadratic shape caused by interactions between normal and shear stresses in the failure criteria. The weaker matrix was the primary load carrying constituent in the σ_y–τ_{xy} loading of the unidirectional (UD) E-glass/LY556/HT907/DY063 lamina. Thus matrix failure determined the final failure envelope. In contrast, the stronger fiber was the primary load carrying constituent in the σ_x–τ_{xy} biaxial loading of the T300/BSL914C lamina. As a result the lamina failure envelope is sharply skewed in the σ_x direction. The failure envelope for a UD E-glass/MY750 lamina under

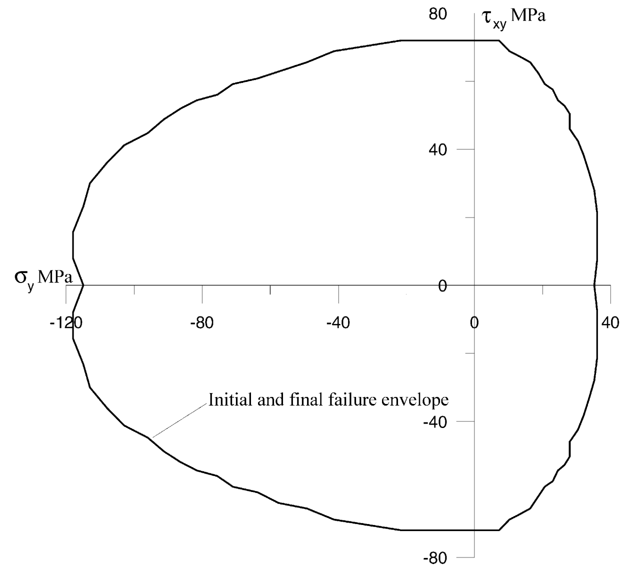

Fig. 4. Failure envelope for a [0°] lamina made from E-glass/LY556/HT907/DY063 under biaxial, σ_y/τ_{xy}, load.

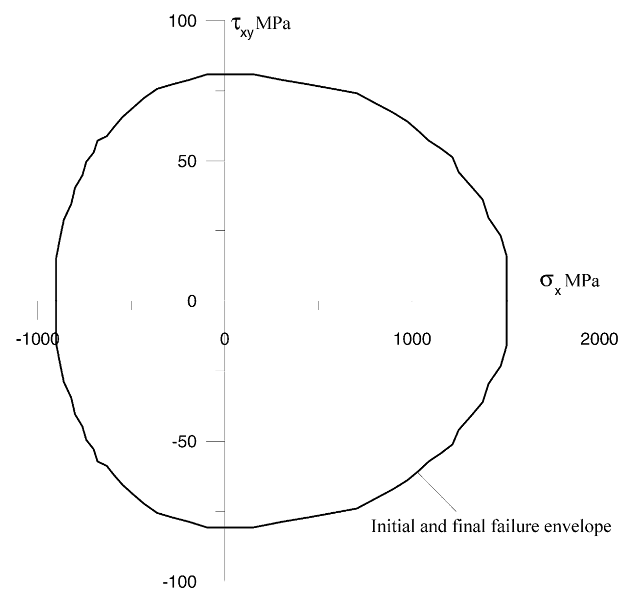

Fig. 5. Failure envelope for a [0°] lamina made from T300/BSL914C under biaxial, σ_x/τ_{xy}, load.

biaxial σ_x/σ_y load is presented in Fig. 6. This envelope was characterized by a distinct transition from fiber to matrix failure resulting in a shape analogous to one that would be produced by a simple maximum stress ${}^{\pm}\sigma^{\pm\pm}\sigma^{\pm}$failure criterion ($_{ijf}/S_{ijf}$ or $_{ijm}/S_{ijm}$). Initial and final lamina failure envelopes in Figs. 4–6 were identical.

Initial and final failure envelopes for an E-glass/LY556/HT907/DY063 $[90°/\pm30°]_S$ laminate under biaxial σ_y /σ_x load are shown in Fig. 7. The final failure envelope exhibits a complex shape because of stress interactions between lamina and changing failure modes

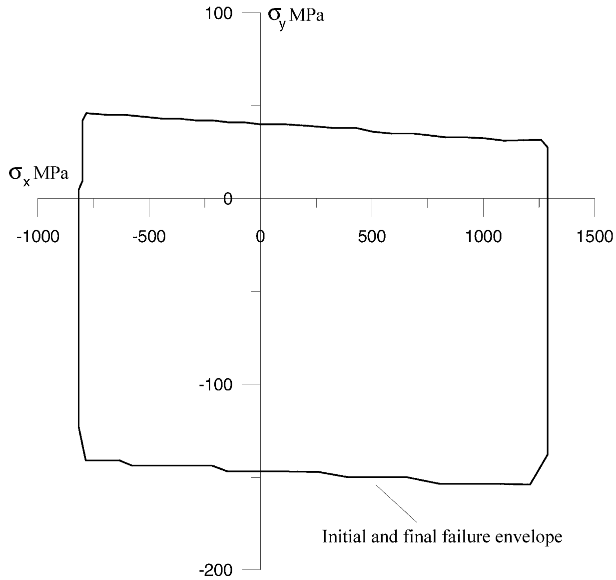

Fig. 6. Failure envelope for a [0°] lamina made from E-glass/MY750/HT917/DY063 under biaxial, σ_y/σ_x, load.

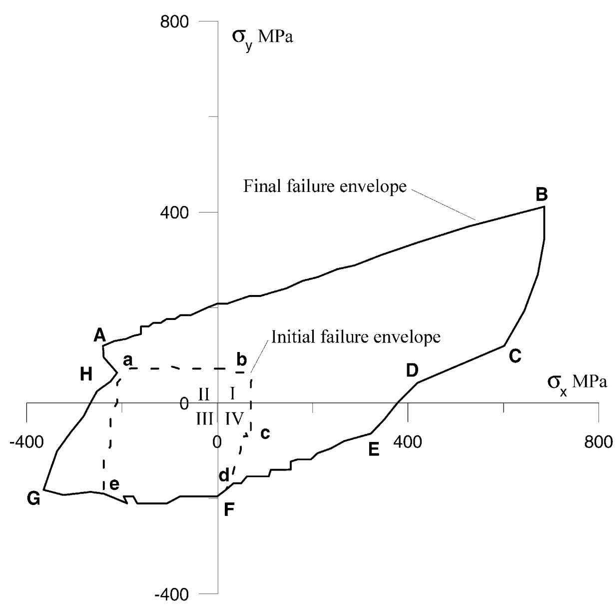

Fig. 7. Failure envelope for a $[90°/\pm 30°]_S$ laminate made from E-glass/LY556/HT907/DY063 under biaxial, σ_y/σ_x, load.

between constituents. Results for the initial and final failure envelopes are summarized in Tables 6 and 7.

The horizontal edge of the initial failure envelope, points a to b, was caused by matrix tensile failure in the $\pm 30°$ lamina. The right edge of the initial failure envelope between points b and c is due to matrix tensile failure 90° lamina. Intermediate damage, in the form of matrix failure, occurred later in the $\pm 30°$ lamina due to combined tensile and shear stresses. Note that in this regime, all matrix in the laminate had failed but the laminate continued to sustain load. Between points c and d, initial matrix damage slowly switches to a combined compression and shear failure in the $\pm 30°$ lamina. From points d to e, the initial and final failure envelopes coincided with compressive matrix failure in the $\pm 30°$ lamina controlling the mode. Initial failure from points e to a was due to matrix compressive failure in the 90° lamina.

The upper edge of the final failure envelope, points A to B began with combined fiber compression-shear failure in the $\pm 30°$ lamina and shifted to fiber tensile failure in the 90° lamina. Catastrophic laminate failure occurred between points B and C due to combined fiber tensile-shear failure in the $\pm 30°$ lamina. Fibers in the 90° lamina were still intact. A change in the failure envelope shape occurred between points C and D where the failure mode switched to *compressive* fiber failure in the 90° lamina (in the *tension–tension* quadrant I) leaving fibers in the $\pm 30°$ lamina intact. Between points D and E, simultaneous fiber failure occurred in the 90° (compressive) and $\pm 30°$ (shear) lamina.

From points E to F, catastrophic laminate failure became increasingly dependent on fiber shear failure in the $\pm 30°$ lamina. From points F to G, the initial and final failure envelopes coincided with compressive matrix failure in the $\pm 30°$ lamina which precipitated fiber compressive failure in the 90° lamina. The mechanism for final failure shifted to fiber shear in the in the 30° lamina for the points G to H.

Initial and final failure envelopes for an E-glass/LY55/HT907/DY063, $[90/\pm 30]_S$ laminate under biaxial, σ_x/τ_{xy}, load are shown in Fig. 8. The failure envelope was symmetric about the σ_x axis. Results for both failure envelopes are summarized in Tables 8 and 9.

Initial laminate damage in quadrant II, between points a and b, was due to compressive matrix failure in

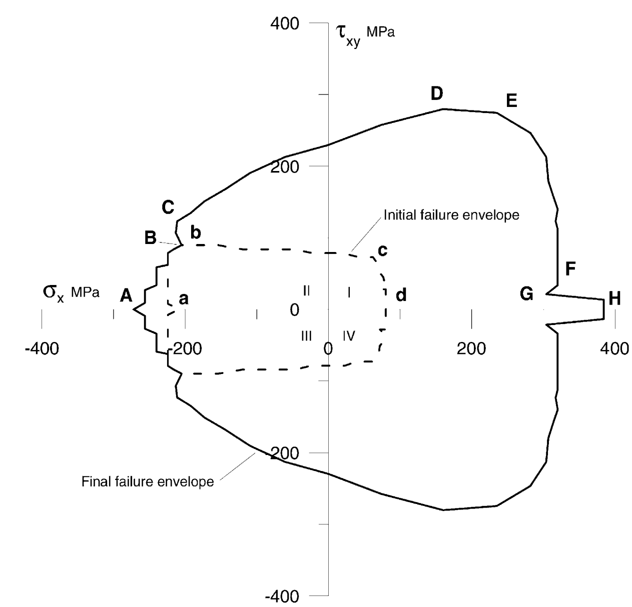

Fig. 8. Failure envelope for a $[90°/\pm 30°]_S$ laminate made from E-glass/LY556/HT907/DY063 under biaxial, σ_x/τ_{xy}, load.

the 90° lamina. Initial failure between points b and c began with combined compression/shear matrix failure in the 90° lamina and tensile/shear matrix failure in the −30° lamina. The failure mode shifted to matrix tension closer to point c. Between points c and d, initial failure was due to tensile matrix failure in the 90 lamina.

The step-like shape of the final failure envelope between points A and B was caused by fiber failure oscillating between the ±30° lamina under combined compressive and shear stresses. In the region about point B, the initial and final failure envelopes coincided. Simultaneous matrix failure in the 90° (compressive) and −30° (tensile) lamina precipitated fiber failure in both the −30° and +30° lamina. From point C to D, the final failure mode transitioned from fiber compressive failure at C to fiber tensile fiber failure at D in the −30° lamina. At point E, the final failure mode switched to tensile fiber failure in the +30° lamina but became increasingly dependent on the shear contribution as one moved towards point F. At point G, final failure began as matrix failure in the −30° lamina, due to combined tensile and shear stresses, which precipitated fiber shear failure in the +30° lamina. A shape change in the failure envelope occurred at point H due to a switch in failure mode to simultaneous fiber failure in the +30° lamina (tensile and shear) and 90° lamina (tensile).

Both initial and final failure envelopes for a AS4/3501-6, $[0°/\pm45°/90°]_S$ laminate under biaxial, σ_y/σ_x, load are shown in Fig. 9. The failure envelope was symmetric about a line through points A and H. Results for the failure envelopes are summarized in Tables 10 and 11.

The initial failure envelope between points a and c was defined by matrix tensile failure in the 90° lamina. At point a, simultaneous matrix failure occurred in all lamina but the laminate retained the ability to sustain load. Later in the load history intermediate laminate damage, in the form of matrix failure in the ±45° lamina, occurred to the right of points b to c due to combined tensile and shear stresses. The initial and final failure envelopes coincided at point c. Failure there was due initially to matrix failure in the 90° (tension) and ±45 (shear) lamina precipitating compressive fiber failure in the 90° lamina.

Final failure between points A and B was due to fiber tensile failure in the 0° lamina. An abrupt change in shape of the failure envelope occurred at point B as the failure mode shifted to fiber shear stress in the ±45 lamina. Between points C and D tensile fiber failure in the 0° lamina and compressive fiber failure in the 90° lamina determined final laminate failure. Fiber shear stresses precipitated failure in the ±45° lamina between points D and E. From points F to H final failure was determined by compressive failure of the fiber in the 90° lamina.

The stress–strain curves for a AS4/3501-6, $[0/\pm45/90]_S$ laminate under uniaxial tension $\sigma_y/\sigma_x = 1/0$ and $\sigma_y/\sigma_x = 2/1$ are shown in Figs. 10 and 11, respectively. Strain jumps in both plots indicated that initial laminate damage occurred due to transverse matrix tensile failures in the 0° lamina. Intermediate damage in the form of matrix failure in the ±45° lamina was caused by combined shear and tensile stresses. Under the $\sigma_y/\sigma_x = 2/1$ load, additional intermediate damage occurred through tensile matrix failure in the 90° lamina. Final failure in both laminates was caused by tensile fiber failure in the 90° lamina.

The E-glass/MY750/HY917/DY063 failure envelope for a $[\pm55°]_S$ laminate under biaxial, σ_y/σ_x, load is

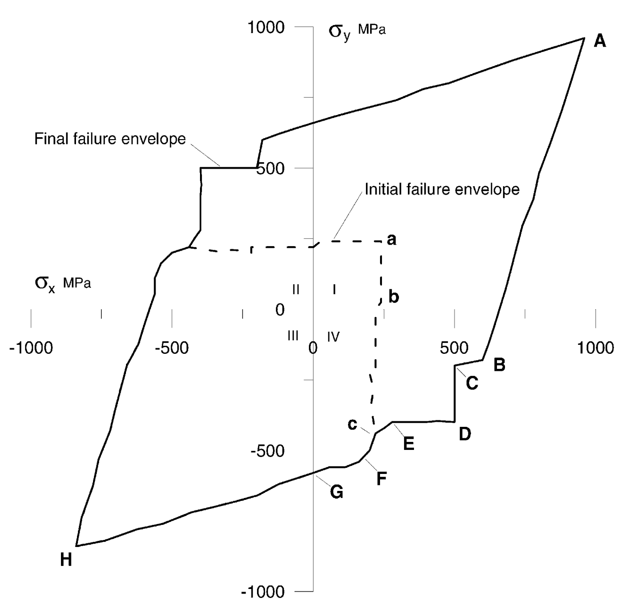

Fig. 9. Failure envelope for a $[0°/\pm45°/90°]_S$ laminate made from AS4/3501-6 under biaxial, σ_y/σ_x, load.

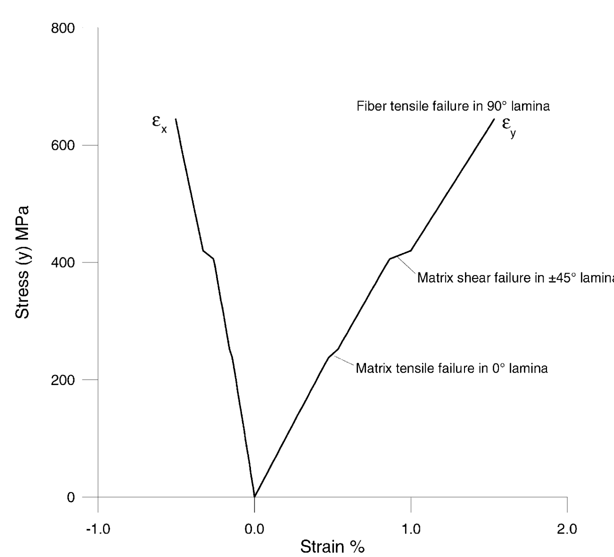

Fig. 10. Stress/strain curves for a $[0°/\pm45°/90°]_S$ laminate made from AS4/3501-6 under uniaxial tension load $\sigma_y/\sigma_x = 1/0$.

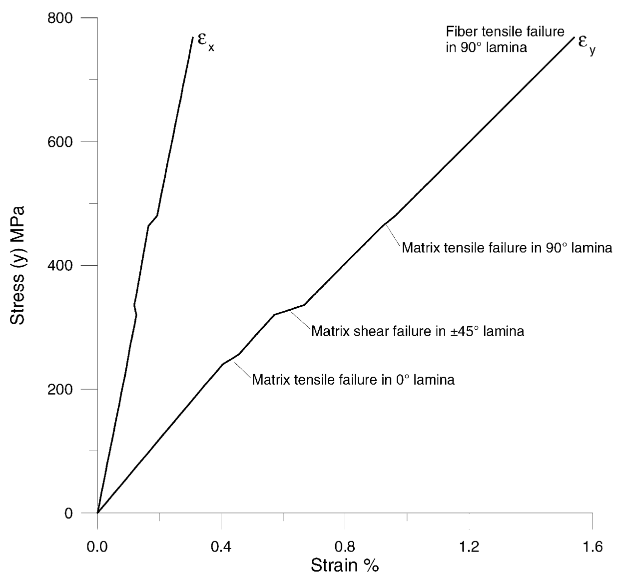

Fig. 11. Stress–strain curves for a $[0°/\pm45°/90°]_S$ laminate made from AS4/3501-6 under biaxial tension load $\sigma_y/\sigma_x = 2/1$.

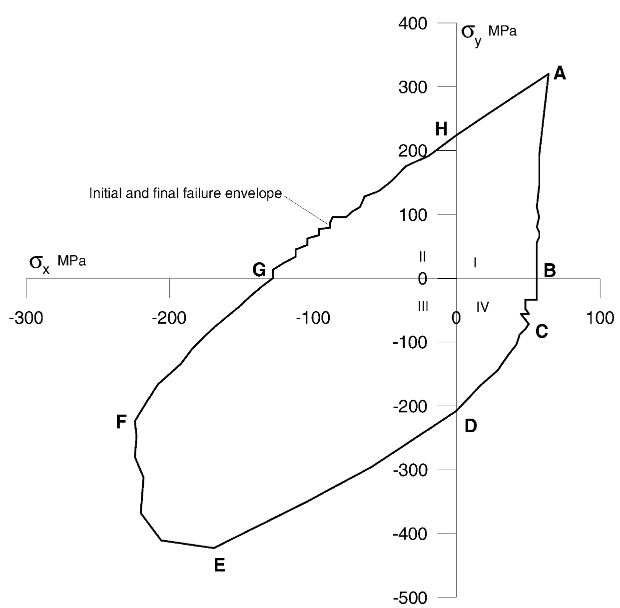

Fig. 12. Failure envelope for a $[\pm55°]_S$ laminate made from E-glass/MY750/HT917/DY063 under biaxial, σ_y/σ_x, load.

shown in Fig 12. Initial and final failure envelopes were identical. Results for the failure envelope are summarized in Table 12.

Tensile matrix failure in all lamina determined failure from points A to B. It is interesting to note that the E-glass/LY55/HT907/DY063, $[90°/\pm30°]_S$ and the AS4/3501-6, $[0°/\pm45°/90°]_S$ laminates under σ_y /σ_x loading also experienced complete matrix failure in quadrant I but continued to load. From points B to D, rising shear stresses combined with tensile stresses to cause matrix failure. The rough envelope edge around point C was due to the manner in which the load was applied, i.e., load step size and σ_y /σ_x ratio, and does not have physical significance. From points D to E fiber failure under combined shear and compressive stress caused laminate failure. Matrix failure due primarily to compressive stresses determined the failure envelope from points E to F. Rising shear stresses combined with the compressive stresses caused matrix failure between points F and G. Failure due to fiber shear stress began at point G and slowly shifted to fiber tensile failure at point H.

Non-linear shear behavior characterized the stress–strain curves of the E-glass/MY750/HY917/DY063, $[\pm55°]_S$ laminate under uniaxial load, σ_y /$\sigma_x = 1/0$, as shown in Fig. 13. Catastrophic laminate failure was caused principally by shear failure of the fibers. Non-linear shear effects did not become significant for the $[\pm55°]_S$ laminate under biaxial loading, σ_y /$\sigma_x = 2/1$, (Fig. 14) because catastrophic matrix tensile failure occurred at relatively low strain levels.

The E-glass/MY750/HY917/DY063 stress strain curves for a $[0°/90°/0]$ laminate under uniaxial load σ_y/$\sigma_x = 1/0$ are shown in Fig. 15. Initial laminate damage due to tensile matrix failure in the 0° lamina occurred at approximately one-third of the ultimate laminate load. This damage is a consequence of the load being applied transversely to the fiber direction in the 0° lamina. Intermediate laminate damage, which was also in the form of matrix tensile failure, occurred in the 90° lamina. This matrix damage was interesting because it occurred in the principal load bearing (σ_{11f}) direction which was aligned with the load. Note that there is no term in the matrix failure criterion, Eq. (19), involving stress σ_{11m}. Therefore this matrix failure was caused by transverse, σ_{22m} and σ_{33m}, stresses arising from Poisson's

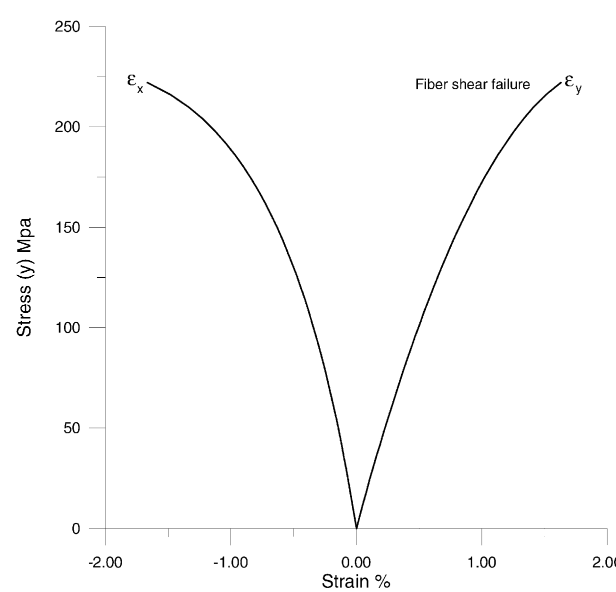

Fig. 13. Stress–strain curves for a $[\pm55°]_S$ laminate made from E-glass/MY750/HT917/DY063 under uniaxial tension load $\sigma_y/\sigma_x = 1/0$.

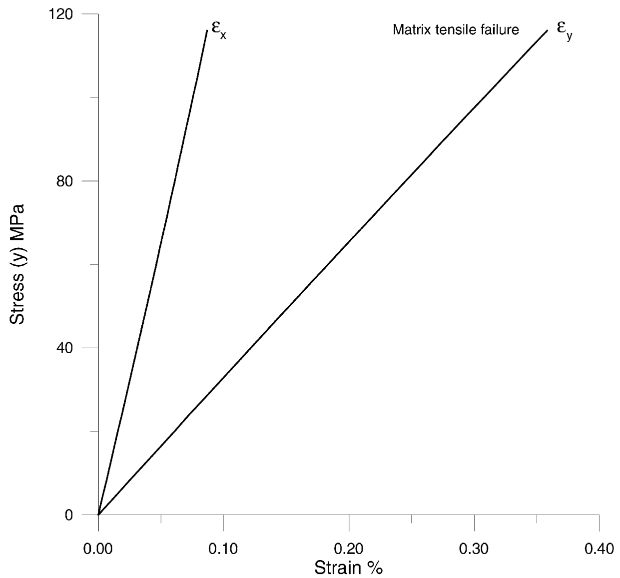

Fig. 14. Stress–strain curves for a [±55°]$_S$ laminate made from E-glass/MY750/HT917/DY063 under uniaxial tension load $\sigma_y/\sigma_x = 2/1$.

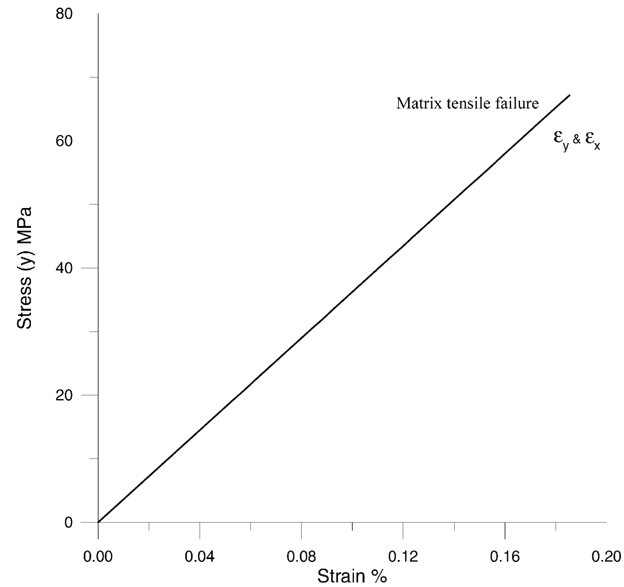

Fig. 16. Stress–strain curves for a [±45°]$_S$ laminate made from E-glass/MY750/HT917/DY063 under biaxial load $\sigma_y/\sigma_x = 1/1$.

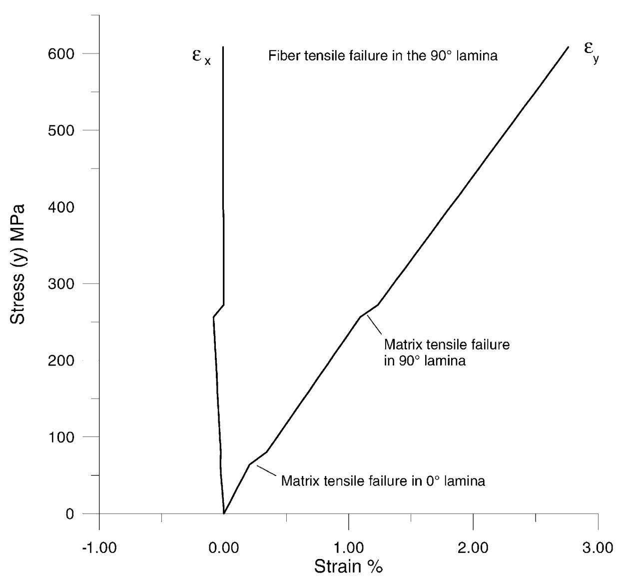

Fig. 15. Stress/strain curves for a [0°/90°/0°] laminate made from E-glass/MY750/HT917/DY063 under uniaxial tension load $\sigma_y/\sigma/$ *it*$>_x = 1/0$.

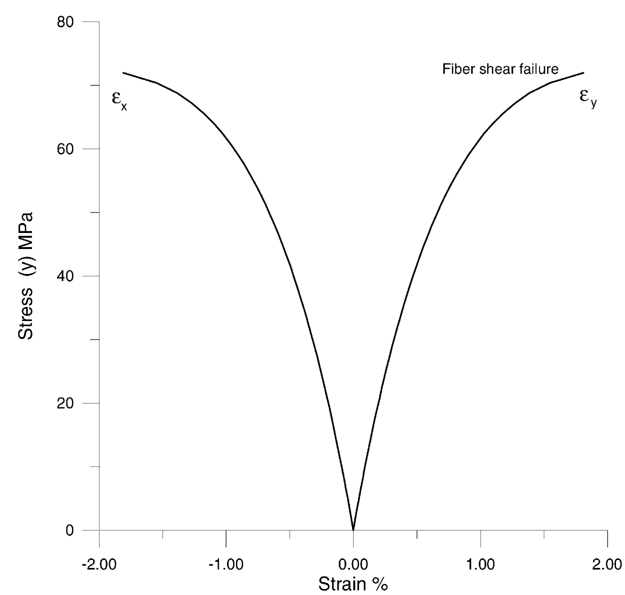

Fig. 17. Stress/strain curves for a [±45°]$_S$ laminate made from E-glass/MY750/HT917/DY063 under biaxial load $\sigma_y/\sigma_x = 1/\text{-}1$.

effect. Tensile fiber failure in the 90° lamina resulted in final laminate failure.

Stress–strain curves for a E-glass/MY750/HY917/DY063, [±45]$_S$ laminate exhibited near linear response under $\sigma_y/\sigma_x = 1/1$ biaxial load as shown in Fig. 16. Catastrophic tensile failure of the matrix occurred before any significant lamina shear stresses developed. In contrast, Fig. 17 shows a highly nonlinear stress–strain response in a [±45°]$_S$ laminate under $\sigma_y/\sigma_x = 1/\text{btl}1$ biaxial load. These shear induced, laminate strains did not become significantly nonlinear until about the 0.5% level which was approximately twice the ultimate laminate strain in the previous $\sigma_y/\sigma_x = 1/1$ load case. Laminate failure under biaxial load $\sigma_y/\sigma_x = 1/-1$ is due to fiber shear failure.

6. Comments on the MCT failure results

The failure load (stress) for individual points on a failure envelope was taken as the value at the beginning of the load step in which failure occurred. The failure value is therefore dependent on the size of the load step but will monotonically converge with decreasing load step size. Generally the lack of smooth failure envelope edges, (e.g., Fig. 8 in the II and III quadrants) is a result of discrete loading ratios and load step size and has no physical significance. Generating a single 2-dimensional failure envelope took on the order of a hundred finite element runs so time constraints prevented detailed convergence of the failure surfaces. Other rough edges, e.g. Fig. 8 on the positive σ_x axis, are due to changes in failure modes from matrix to fiber and may have physical significance.

Establishing initial, intermediate, and final failure envelopes serves to highlight the importance of assessing constituent damage in a structural analysis. The practical implications of the different failure surfaces are in establishing allowable stress levels in a composite design, e.g., at what degree of laminate damage is composite 'failure' deemed to have occurred?

The MCT approach to failure analysis requires identifying constituent failure modes from composite test data. Identifying the constituent that precipitates failure in longitudinal and transverse lamina tension and compression tests is intuitive and straightforward, i.e., fiber failure for longitudinal loads and matrix failure for transverse loads. Identifying the constituent leading to shear failure is more problematic, as non-catastrophic matrix and fiber damage begins well before ultimate composite strength is achieved [23]. Ultimate constituent shear strengths have previously been determined by utilizing nonlinear regression analysis of load cases involving varying amounts of combined normal and shear stresses [5]. Specifically, we make an educated guess as to each constituents shear strength and then use that data to predict lamina failure in off-axis tension tests. Using the experimentally determined lamina failures and our initial guess, we iterate with additional guesses until failure predictions based on constituent shear failure produce composite failures that more or less agree with the experimental data. Armed with these semi-empirical constituent shear strengths we have increased confidence in analysis of more complex problems involving shear.

Data from off-angle, balanced, symmetric laminates, $[\pm\theta]_S$, provide an excellent basis for determining a best fit determination of failure parameters S_{12m}, S_{23m}, and S_{12f}. Hence, some of the laminates analyzed as part of this exercise would, in a normal case, be used as inputs to the failure prediction process.

Thermal effects due to curing,were neglected in all analyses conducted as part of the failure exercise. However, as noted previously, in situ material properties, as determined from finite element micromechanics, were utilized in this failure analysis. Differences between the in situ properties used herein and those provided by the organizers may be explained in part by residual thermal stresses. MCT can account for post-cure thermal effects through the thermal vector, $\{a\}$, in Eq. (10).

MCT's handling of thermal effects can be demonstrated using the E-glass/MY750/HT917/DY063 composite as an example. The organizers provide a stress-free reference temperature of 120 °C for this material. We assume that uniaxial testing used to determine lamina composite tensile strengths occurred at 20 °C. Conducting an MCT analysis of the uniaxial strength test, with a $\Delta T=-100$ °C, we backed out the temperature adjusted normal constituent tensile strengths shown in Table 13. A negative ΔT produces internal matrix tensile stresses. Accounting for this internal tensile load has the net effect of increasing matrix tensile strength and reducing matrix compressive strength. A $\Delta T=-100$ °C has no significant effect on the E-glass fiber normal strengths. Next we reanalyzed test case numbers 12 and 13, i.e., $\sigma_y/\sigma_x=1/0$ loading of the $[\pm 45°]_S$ and the [0°/90°/0°] laminates, again assuming a $\Delta T=-100$ °C. The MCT program applies ΔT in its entirety as a uniform temperature in the first load step.

In the thermal analysis of the [0°/90°/0°] laminate, shown in Fig. 18, the higher matrix CTE (compared to the fiber CTE) causes the 0° lamina matrix to attempt to

Table 13
Effect of ΔT on constituent normal strengths for E-glass /MY750/HY917/DY063

Component	Strength (MPa)	
	$\Delta T=0$ °C	$\Delta T=-100$ °C
$^{+}S_{11f}$	2040	2040
$^{-}S_{11f}$	−1275	−1275
$^{+}S_{22m}$	31.5	42.0
$^{-}S_{22m}$	−114.3	−103.8
$^{+22}S_{33m}$	4.63	15.09
$^{-22}S_{33m}$	−16.8	−6.3

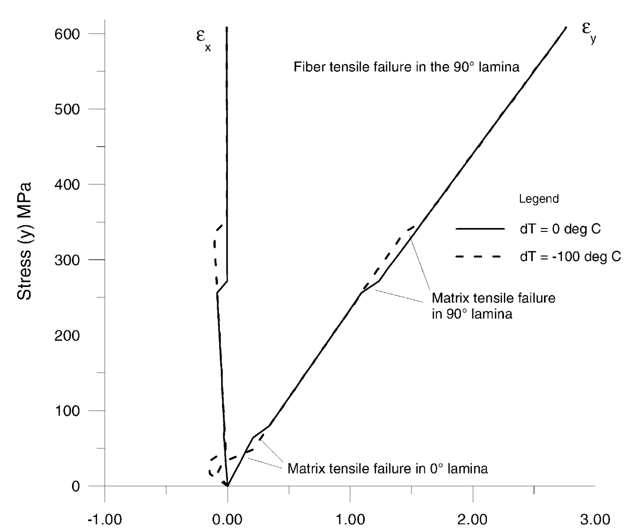

Fig. 18. Stress–strain curves for a [0°/90°/0°] laminate made from E-glass/MY750/HT917/DY063 under uniaxial tension load $\sigma_y/\sigma_x=1/0$ and $\Delta T=-100$ °C.

Table 14
Effect of ΔT on ultimate laminate strength

Laminate	Strength (MPa)	
	$\Delta T = 0$ °C	$\Delta T = -100$ °C
$[\pm 45°]_S$	68.8	38.4
$[0°/90°/0°]$	624	624

Table 15
Thermally induced matrix stresses in each lamina for $\Delta T = -100$ °C

Laminate	Lamina stress (MPa)		
	σ_{11m}	σ_{22m}	σ_{33m}
$[0°]_N$	27.1	10.5	10.5
$[\pm 15°]_S$	26.9	13.0	11.2
$[\pm 30°]_S$	28.4	19.5	12.5
$[\pm 45°]_S$	30.5	24.7	12.5
$[\pm 60°]_S$	28.4	19.5	12.5
$[0°/90°]_S$	30.5	24.7	12.5

contract more, in the transverse (global y) direction, than the 90° lamina fibers allow. This lamina interaction induces matrix tensile stresses that partially offset the higher matrix tensile, temperature adjusted, strength. The combined thermal and mechanical matrix tensile stresses cause a 0° lamina matrix tensile failure to occur earlier than the case of $\Delta T = 0$. Later in the load history, the higher matrix tensile, temperature adjusted, strength causes a 90° lamina matrix tensile failure to occur at a higher laminate load than in the case of $\Delta T = 0$. The [0°/90°/0°] laminate ultimate strength, shown in Table 14, is fiber dominated and thus does not change with $\Delta T = -100$ °C.

The data listed in Table 14 show that the matrix dominate ultimate strength of the $[\pm 45°]_S$ laminate is significantly reduced due to the combination of thermal and mechanical induced matrix tensile stresses. As in the case of the $[0°/90°]_S$ laminate, the orthogonal orientation of the ±45 lamina fibers restrains the matrix thermal contraction inducing high matrix tensile stresses. For comparison purposes, Table 15 presents the magnitudes of thermally induced matrix tensile stresses in several laminate cases.

Clearly thermally induced residual cure stresses can be important but in the absence of precise knowledge these stresses induced during the cure process, accounting for thermal processing effects is a questionable endeavor.

7. Concluding remarks

MCT is a fully 3-dimensional failure prediction methodology intended to efficiently bring constituent information to bear on the analysis of general composite structures. Because failure of composite laminates begins at the constituent level, the constituent information provided by MCT has tremendous value. Accurate predictions of constituent level failure, within the framework of the finite element method, enables development of a progressive failure analysis for general structures. Permitting only one constituent to fail while keeping the others intact allows load redistribution to other parts of the structure as well as to the remaining constituents. Material failure can be tracked as it occurs region by region. The stiffness and strength of damaged areas can be reduced without necessarily declaring total structural failure. This approach has not been incorporated in general design practice in the past because constituent information was generally unavailable in standard finite element analysis.

Acknowledgements

The research reported herein was supported by the In-house Laboratory, Independent Research program at the Naval Surface Warfare Center, Carderock Division and by the Office of Naval Research under Grant N00014-97-1-1081.

References

[1] Aboudi J. Micromechanical analysis of the strength of unidirectional fiber composites. Compos Sci Technol 1988;33:79.
[2] Pecknold DA, Rahman S. Application of a new micromechanics-based homogenization technique for nonlinear compression of thick-section laminates. In: Groves SE, Highsmith AL, editors. Compression response of composite structures, ASTM STP 1185. Philadelphia: American Society for Testing and Materials; 1994. p. 34.
[3] Rahman S, Pecknold DA. Micromechanics-based analysis of fiber-reinforced laminated composites. Civil Engineering Studies, UILU-ENG-92-2012, Department of Civil Engineering, University of Illinois, Urbana-Champaign, September 1992.
[4] Kwon YW, Berner JM. Micromechanics model for damage and failure analyses of laminated fibrous composites. Eng Fracture Mech 1995;52(2):231.
[5] Mayes JS. Micromechanics based failure analysis of composite structural laminates. Naval Surface Warfare Center, Carderock Division Report, NSWCCD-65-TR–1999/15, September 1999.
[6] Garnich MR, Hansen AC. A multicontinuum theory for thermal-elastic finite element analysis of composite materials. J Compos Mater 1997;31(1).
[7] Garnich MR, Hansen AC. A multicontinuum approach to structural analysis of linear viscoelastic composite materials. J Appl Mech 1997;64:795.
[8] Agarwal BD, Broutman LJ. Analysis and performance of fiber composites, 2nd ed. New York: John Wiley & Sons; 1990.
[9] Hill R. Theory of mechanical properties of fibre reinforced materials—I. Elastic behaviour. J Mech Phy Solids 1964;12:199–212.
[10] Garnich, M. R. 1996. A multicontinuum theory for structural analysis of composite materials. PhD dissertation, University of Wyoming.
[11] Brockenbrough JR, Suresh S, Wienecke HA. Deformation of metal matrix composites with continuous fibers: geometrical effects of fiber distribution and shape. Acta Metall Mater 1992.

[12] Soden PD, Hinton MJ, Kaddour AS. Lamina properties, lay-up configuration and loading conditions for a range of fibre-reinforced composite laminates. Compos Sci Technol 1998;58(7):1011.

[13] Gibson RF. Strength of a continuous fiber-reinforced lamina. In: Principles of composite material mechanics. New York: McGraw-Hill; 1994. p. 108.

[14] Nahas MN. Survey of failure and post-failure theories of laminated fiber-reinforced composites. J Compos Technol Res 1986;8:138–53.

[15] Gol'denblat I, Kopnov VA. Strength of glass reinforced plastics in the complex stress state. Mekhanika Polimerov 1965;1:70 [English translation: Polymer Mechanics, 1966, 1, 54]..

[16] Tsai SW, Wu EM. A general theory of strength for anisotropic materials. J Compos Mater 1971;5:58.

[17] Hoffman O. The brittle strength of orthotropic materials. J Compos Mater 1967;1:200.

[18] Hashin Z. Failure criteria for unidirectional fiber composites. J Appl Mech 1980;47:329.

[19] Hansen AC, Blackketter DM, Walrath DE. An invariant-based flow rule for anisotropic plasticity applied to composite materials. J Appl Mech 1991;58:881.

[20] Pipes RB, Cole BW. On the off-axis strength test for anisotropic materials. J Compos Mater 1973;7:246.

[21] Narayanaswami R, Adelman HM. Evaluation of the tensor polynomial and hoffman strength theories for composite materials. J Compos Mater 1977;11:366.

[22] Mayes JS. Multicontinuum failure analysis of composite structural laminates. PhD dissertation, University of Wyoming, 1999.

[23] Gipple K, Camponeschi ET. The influence of material nonlinearity and microstructural damage on inplane shear response of carbon/epoxy composites. Advanced Composites Lett 1992; 1(1):9.